Vortex Lattice CFD Application and Modeling Validation for Ground Effect Aircraft

KARL ZAMMIT, HOWARD SMITH, NOEL SIERRA LOBO, IOANNIS K. GIANNOPOULOS
Centre of Excellence for Aeronautics,
School of Aerospace, Transport and Manufacturing,
Cranfield University,
Cranfield, MK43 0AL
UNITED KINGDOM

Abstract: - This paper explores the application of vortex lattice computational fluid dynamics method capability to model aircraft flight near to ground, utilizing the ground effect. Computational results were correlated with existing analytic formulations and benchmarked against experimental data from the public domain. A case aerodynamics design study was formed, based on the Russian A-90 Orlyonok Ekranoplan wing. The study provided a verification and a validation step towards advancing ground effect aircraft turnaround conceptual and preliminary design time, using the rapid aerodynamics results generation vortex lattice CFD method.

Key-Words: - Ekranoplan, CFD, Vortex Lattice method, AVL, Flight Ground Effect, A-90 Orlyonok.

Received: January 29, 2023. Revised: November 18, 2023. Accepted: December 16, 2023. Published: February 9, 2024.

1 Introduction

Wing-in-ground, WIG-craft, are aircraft vehicles that fly near a surface, mostly above water surfaces. The vehicles make use of the Ground Effect (GE) being the increased lift curve slope and reduced induced drag of the main lifting surfaces, [1].

GE effects are broadly understood as wing-span and wing-chord effects, [1]. The wing-span dominant GE is directly related to a reduction in the induced drag, which is proportional to the wing's spanwise length. When a wing is close to the ground, there is insufficient space for the full development of wingtip vortices. Consequently, air pressure leakage from under the wing to the upper section is reduced. Additionally, the ground's effect pushes the vortices outwards, effectively artificially increasing the wing's aspect ratio beyond its geometric value.

The wing-chord dominant GE involves an increase in static pressure of the oncoming air beneath the wing, which could be further enhanced by utilizing wingtip side plates, [2]. The chord-dominant GE enables the wing to generate more lift per unit area, resulting in a higher lift coefficient for the same power input, [1].

The distance between the wing and the ground influences many of the effects experienced during flight. Three distinct models have emerged from the literature, each focused on a specific height zone above the surface, [3], [4]. The first zone is the operational region between the surface boundary and a flight height corresponding to 20% of the wing-chord length. In this In-Ground-Effect region (IGE), the flow experiences significant constriction in the vertical direction, leading to a predominantly two-dimensional flow with restricted vertical freedom. The second zone is referred to as the region between one wing-chord length and ten wing-span lengths above the ground. Within this zone, the wing's span dominates the model. Inviscid flow models are commonly employed in this region and demonstrate a marginal increase in the Lift to Drag ratio (L/D), compared to the Out-of-Ground-Effect (OGE) flight. A combination of the two models is necessary to accurately capture the aerodynamic behavior of wings operating in the region between 20% - 100% of chord length, [4]. Above ten wing-span lengths, free-flight models used in conventional aerodynamic theory for aircraft design are applicable.

Distinct wing designs can be observed for WIG craft throughout history. Russian Ekranoplans such as the Korabl Market, the A-90 Orlyonok, and the Lun-class craft, used a low aspect ratio straight wing with minimal taper and twist. In contrast, the German RFB X-114 and Chinese XTW had wings with a significantly low aspect ratio, a very high taper ratio, slightly sweptback leading and trailing edges, and an appreciably large wing setting angle. More recent WIG craft designs include the soon-to-enter service Viceroy Seaglider by Regent, which has a noticeably different wing planform with a high

aspect ratio and quasi-organic shape. A part of the aviation industry has shown interest in the development of WIG-craft. The study below showcases the use of computational time-efficient aerodynamics tools capable of rapid design evaluation, mostly applicable to the early aerodynamic iterative aircraft design.

2 Ground Effect Flight

At the early aircraft design stages, namely at the conceptual and initial design stages, a parametric design space of all the aircraft features to be determined is explored, for configuring the most important variables from the design perspective. To reach an optimum set of design parameters framed by several constraints, usually rapid evaluation, lower fidelity analysis computational tools are employed. There are key aspects to be considered upon selecting such tools, namely, time efficiency and results accuracy relative to the maturity level of the design stage.

The study herein, aimed at providing validation and verification insights in the utilization of Vortex Lattice computational fluid dynamics method (VLM) applied to WIG-craft. For that purpose, various analytical formulations and experimental data were benchmarked against the numerically VLM derived solutions.

2.1 Analytical Formulations

A thorough review of the analytical formulations of a wing IGE shed light on various metrics for efficiency comparison. The equations listed below-maintained adherence to the operational parameters analyzed in [5]. The main parameter utilized is the ratio of the height of the mean aerodynamic chord from the ground {h_c} to the wingspan {b}, denoted herein by $h_{\bar{c}}/b$.

2.1.1 Induced Drag GE Reduction Factor

Derived from reference [6], various closed-form relations are available in literature that can be used to estimate the effect of IGE flight on the induced drag. The drag reduction factor, [7], shown in eq.(1), is the ratio of the induced drag in IGE flight condition versus the OGE one. The equations presented in [8], [9] for wings IGE are re-iterated below in eq.(2) and eq.(3).

$$K_1 = \frac{(C_{D,i})_{IGE}}{(C_{D,i})_{OGE}} \tag{1}$$

$$K_1 = 1 - \left(\frac{2e}{\pi^2}\right) \ln\left[1 + \left(\frac{\pi}{4}\right)\left(\frac{1}{2\,h_{\bar{c}}/b}\right)^2\right] \tag{2}$$

$$K_1 = \frac{1 - \left(\frac{2}{\pi}\right) + \left(\frac{16\,h_{\bar{c}}/b}{\pi}\right)^2}{1 + \left(\frac{16\,h_{\bar{c}}/b}{\pi}\right)^2} \tag{3}$$

It has been noted in [10], that eq.(3) tends to significantly underpredict the induced drag for $h_{\bar{c}}/b < 1$.

2.1.2 Induced Drag GE Influence Ratio

The induced drag coefficient over the lift coefficient squared IGE to that OGE shown eq.(4), is referred to as the induced-drag ground effect influence ratio, [10].

$$K_2 = \frac{\left(C_{D,i}/C_L^{\,2}\right)_{IGE}}{\left(C_{D,i}/C_L^{\,2}\right)_{OGE}} \tag{4}$$

Reference [10], derived several closed-form relations to estimate the induced drag and lift coefficients IGE. Starting from a review of earlier equations, their first contribution improved the approximation given in [7], by slightly modifying the coefficients in eq.(5).

$$K_2 = 1 - e^{\left[-4.01\left(h_{\bar{c}}/b\right)^{0.717}\right]} \tag{5}$$

Equations (6) and (7), followed as a closed-form relation for the induced drag IGE influence ratio, verified via a comparison with results obtained from numerical lifting-line solutions.

$$K_2 = 1 - \delta_D e^{\left[-4.74\left(h_{\bar{c}}/b\right)^{0.814}\right]} - \left(h_{\bar{c}}/b\right)^2 e^{\left[-3.86\left(h_{\bar{c}}/b\right)^{0.758}\right]} \tag{6}$$

$$\delta_D = 1 - 0.157\left(R_T^{\,0.775} - 0.373\right)\left(R_A^{\,0.417} - 1.27\right) \tag{7}$$

Noting that eq.(6) agrees mostly only at small angles of attack, the correction factor {β_D} in eq.(8) is applied by multiplying the result of eq.(6) to

increase the accuracy for higher angles of attack, [10].

$$\beta_D = 1 + \frac{0.0361 {C_L}^{1.21}}{{R_A}^{1.19} \left({h_{\bar{c}}}/{b}\right)^{1.51}} \tag{8}$$

2.1.3 Lift GE Influence Ratio

The ratio of the induced drag coefficient over the lift coefficient squared IGE to that OGE shown in eq.(9), is referred to as the induced-drag ground effect influence ratio, [10].

$$K_3 = \frac{[C_L(\alpha)]_{IGE}}{[C_L(\alpha)]_{OGE}} \tag{9}$$

Derived in [10], K_3 is presented in eq.(10).

$$K_3 = 1 + \delta_L \frac{288 \left({h_{\bar{c}}}/{b}\right)^{0.787} e^{\left[-9.14\left({h_{\bar{c}}}/{b}\right)^{0.327}\right]}}{{R_A}^{0.882}} \tag{10}$$

$$\delta_L = 1 - 2.25\left({R_T}^{0.00273} - 0.997\right)\left({R_A}^{0.717} + 13.6\right) \tag{11}$$

A correction factor to improve the accuracy at high lift coefficients was also suggested, [10], and given in eq.(12).

$$\beta_L = 1 + \frac{0.269 {C_L}^{1.45}}{{R_A}^{3.18} \left({h_{\bar{c}}}/{b}\right)^{1.12}} \tag{12}$$

ESDU 72023, [11], presented another equation formed from the contribution of several studies, such as that documented in [12], to estimate the increment to the lift coefficient due to the ground effect given by eq.(13). The derivation of each parameter may be found in the ESDU method, [11].

$$\frac{\Delta C_L}{(C_L)_{OGE}} = \frac{1}{1 - \left(\frac{a\sigma}{\pi A}\right)} \left\{ \frac{a\sigma}{\pi R_A} + r \left[\frac{N}{\left(1 + {\tau N (C_L)_{OGE}}/{1 - \frac{a\sigma}{\pi R_A}}\right)^2} - 1 \right] \right\} \tag{13}$$

For non-dimensional ground flight distance of $h_{\bar{c}}/b < 1$ and for small free-air lift coefficients, experimental evidence highlights the need to account for the wing thickness when evaluating the GE on lift, [11]. The approximation for the wing thickness correction given by eq.(14), is suggested in the absence of experimental data.

$$\left.\begin{array}{ll} \Delta C_{L,t} = r[1 - 1.4(C_L)_{OGE}]\Delta C_{L,t_0} & (C_L)_{OGE} < 0.7 \\ \Delta C_{L,t} = 0 & (C_L)_{OGE} \geq 0.7 \end{array}\right\} \tag{14}$$

It is important to note that, in the context of the presented ESDU method, eq.(14) assumes the retraction of any high-lift devices at the same aircraft incidence

2.2 Computational Tools

Various aerodynamic computational solvers can be employed in the design synthesis of aircraft design. The Navier-Stokes equations with turbulence modeling could potentially offer the most realistic prediction of the aerodynamic forces and moments for complex geometries, [13]. Implementing Navier Stokes solvers can be quite computationally time inefficient, particularly when such tools are implemented within multivariable design synthesis optimization processes, [14].

The inviscid Euler equations, derived by eliminating diffusion terms from the Navier-Stokes equations, allow for the solution of rotational, non-isentropic shock flows, predicting well enough phenomena such as wave drag, [15]. Nonetheless, Euler solvers cannot predict viscous drag and are computationally expensive due to the need to solve at least five coupled first-order partial differential equation,s [16].

A need for lower fidelity yet faster aerodynamic solvers is present, provided by non-linear and linear potential flow solvers. Linear potential flow codes based on the Laplace equations, are solved using panel or Vortex Lattice Method (VLM).

Panel methods provide an approximate solution distributed over the geometry's surface and can be enhanced by higher-order modeling and the inclusion of lifting capability, unsteady flows, and boundary layer effects, [17]. VLMs solve the Laplace potential flow equations using singularities on the mean surface of the geometry, [18]. However, VLMs and panel methods cannot handle turbulence, viscosity, and flow separation, [17], [18]. Nonetheless, VLMs are computationally efficient and are currently widely used in the aircraft

conceptual and initial design phases, [18], as well as in other similar fields of engineering, [19].

2.2.1 Short Survey on VLM Aerodynamic Tools

For the present study, several open-source panel methods and VLMs were surveyed, including WINGBODY, PANAIR, XFLR5, and the Athena Vortex Lattice, AVL software platforms.

WINGBODY [20], is a panel method useful for simple 3D geometry analysis at subsonic and supersonic conditions, though it lacks modeling capabilities for wing twists and complex geometries with multiple sections.

PANAIR [21], is a higher-order panel method that supports the analysis of complex 3D geometries in subsonic and supersonic aerodynamics. However, it has limited aero-foil options and cannot predict flow characteristics accurately for configurations with different total pressures. Moreover, it requires a commercial pre-processor for modeling flight control surfaces.

XFLR5 [22], is an aerodynamic suite that incorporates both VLM and 3D panel methods and allows the modeling of more complex configurations at various angles of attack. Nevertheless, it involves complicated geometric manipulation to swiftly model control surfaces and lacks explicit stability and control derivatives.

The AVL method, [23], is based on VLM. It supports aerodynamic analysis of simple and complex geometries at subsonic conditions. It offers quasi-steady flow analysis and includes compressibility effects. AVL's open-source nature allows for remote operation, and it effectively investigates geometric and aerodynamic twists and control surface deflections, providing stability and control derivatives without additional manipulation, [17], [23]. To capture the effects of ground effect, AVL has the capability of setting up a symmetry plane whereby while the aerodynamic implications of ground effect are taken into account, the forces are not calculated on the image surfaces. This method is similar in principle to the method in [24], where the study explores reducing induced drag in wings by employing an imaging method to estimate the drag reduction factor.

2.2.2 Experimental Verification

The VLM verification exercise was based on the findings of [5], which provided wind tunnel experimentally derived aerodynamic properties of a 3D finite rectangular wing of NACA0012 profile at relatively lower Reynold's numbers. Although a symmetrical aerofoil profile is generally not recommended for WIG-craft to avoid possible suction towards the ground, [1], the NACA0012 profile was used due to the lack of other publicly available test data.

An identical wing to the experimental survey was constructed in AVL, having a chord of 63mm and a span of 400mm. The flight parameters were set at a flow velocity of V_∞=20ms^{-1}, air density of ρ_∞=1.225kgm^{-3}, and viscosity of μ_∞=1.75×10-5kgm^{-1}s^{-1}, which resulted in Re≈8.8×10^{-5}. The experimental study was performed for angles of attack $\{\alpha\}$ between -8° to 18°, at five non-dimensional heights $h\bar{c}$/b equal to 0.4, 0.6, 0.8, 1.0 and 1.5. The value of $h\bar{c}$/b at 1.5 was considered OGE by [5].

Results convergence testing was conducted for the numerical VLM models generated grids via systematic refinement of the discretisation of the wing, to ensure that the solution is independent of the element size. The results of the mesh sensitivity are shown in Figure 1, Figure 2, Figure 3, Figure 4, Figure 5 and Figure 6, in terms of calculated lift, drag, and moment coefficients $\{C_L, C_D, C_m\}$ for the NACA0012 3D VLM modeled aerofoil section, versus a number of elements used and for angles of attack $\{\alpha\}$ from -5° to +5°. The chart abscissa values are the coefficients residuals, namely the actual coefficient subtracted from the average value of the coefficients calculated from the sum of the tests for various numbers of elements at that angle of attack. The charts are interpreted in terms of the coefficient attaining a constant value after a certain number of elements used in the mesh, an indication of the results being mesh independent, as well as the magnitude of the attained value being a measure of the residual error. The numerical tests were performed for OGE as well as for IGE at $h\bar{c}$/b =0.4.

The numerical mesh discretization sensitivity testing, Figure 1, Figure 2, Figure 3, Figure 4, Figure 5 and Figure 6, showed convergence of the results for the coefficients in question after a certain number of elements and above. For the IGE scenario, a slightly increased number of elements were required compared to OGE cases.

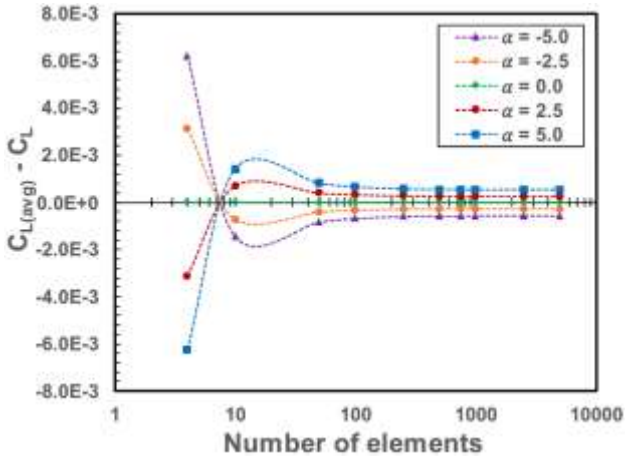


Fig. 1: NACA0012, OGE residuals C_L

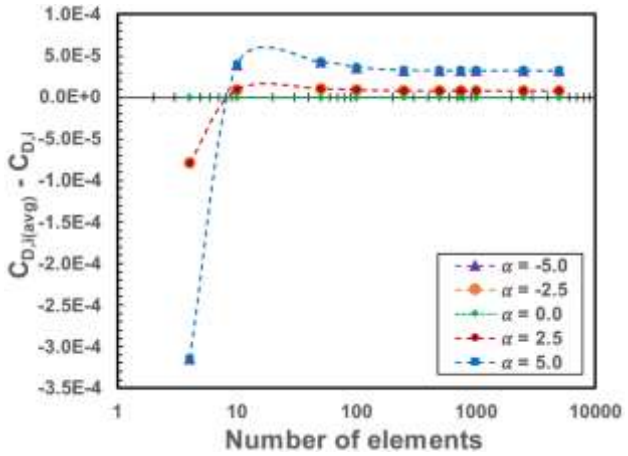


Fig. 2: NACA0012, OGE residuals $C_{D,i}$

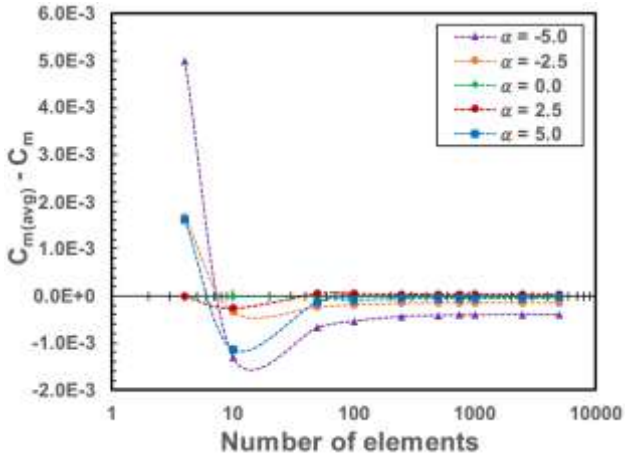


Fig. 3: NACA0012, OGE residuals C_m

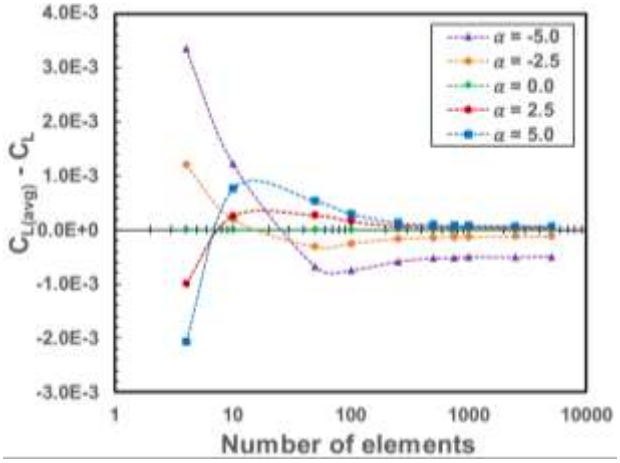


Fig. 4: NACA0012, IGE ($h\bar{c}$/b=0.4) residuals C_L

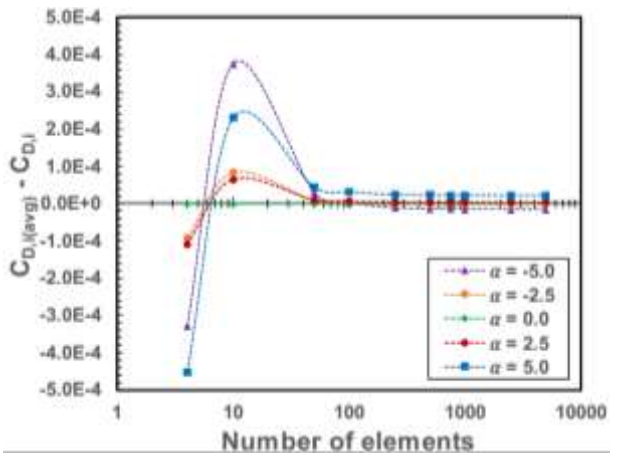


Fig. 5: NACA0012, IGE ($h\bar{c}$/b=0.4) residuals $C_{D,i}$

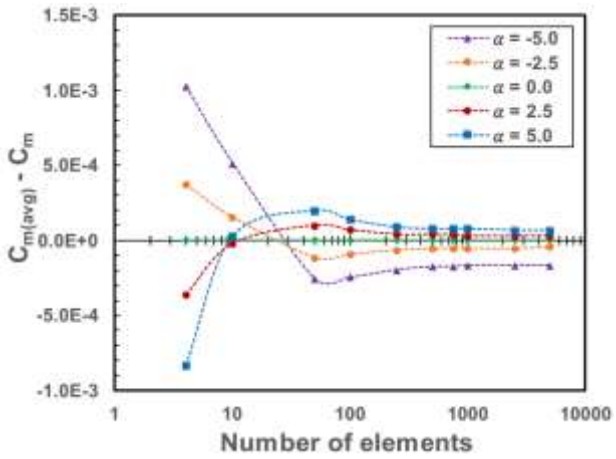


Fig. 6: NACA0012, IGE ($h\bar{c}$/b=0.4) residuals C_m

3 Results

3.1 Analytic Formulations Correlations

The induced drag reduction factor, K_1, the induced drag ground effect influence ratio, K_2, and the lift ground effect influence ratio, K_3, of para 2.1 herein, were evaluated and displayed in Figure 7, Figure 8

and Figure 9. The results refer to the NACA0012 wing section described in para 2.2.2 herein, as a function of the nondimensional height, h$\bar{c}$/b. The numerical results from AVL were superimposed on the figures as well.

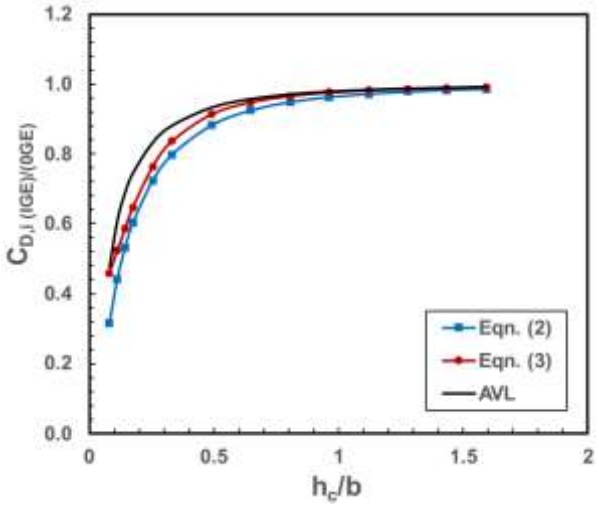


Fig. 7: NACA0012, K_1

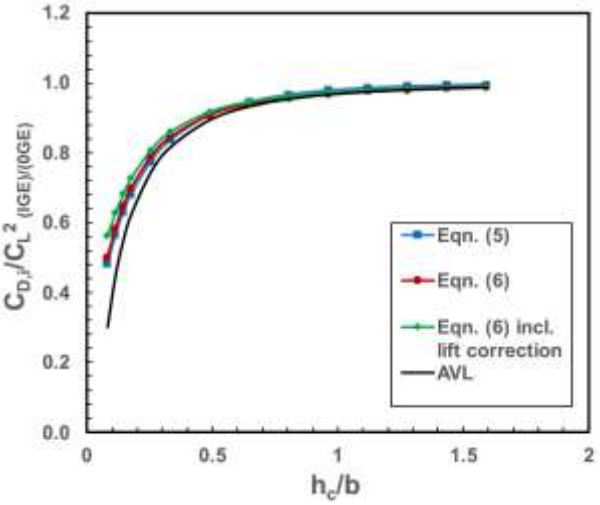


Fig. 8: NACA0012, K_2

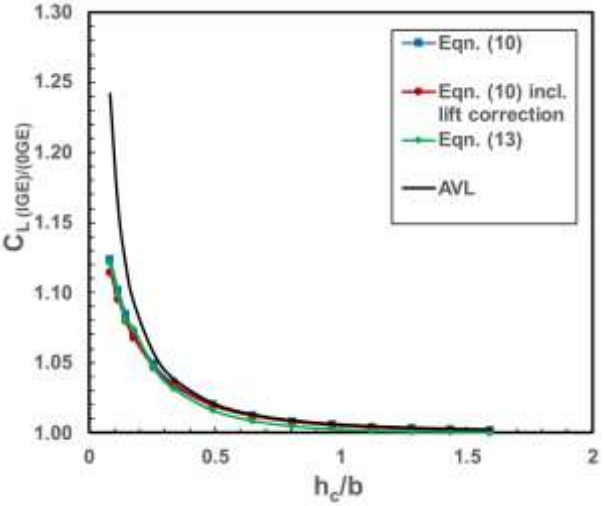


Fig. 9: NACA0012, K_3

It can be observed that the results generated by the AVL VLM method correlate relatively well with the results from analytical formulations, for higher values of the non-dimensional distance from the ground. The closer the distance to the ground, the larger the deviation of the parameters in question.

3.2 Experimental Results Benchmark

The variation of lift and drag coefficients from the work of [5], were benchmarked against AVL results and are shown in Figure 10 and Figure 11. Given that AVL is recommended for small angles of attack, [23], simulations run in the range $-8° \leq \alpha \leq +8°$ and for the non-dimensional height off the ground plane dictated in para 2.2.2.

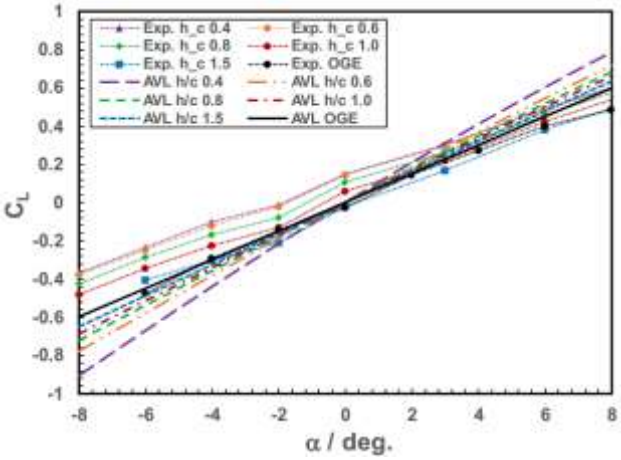


Fig. 10: NACA0012, C_L, experimental vs AVL

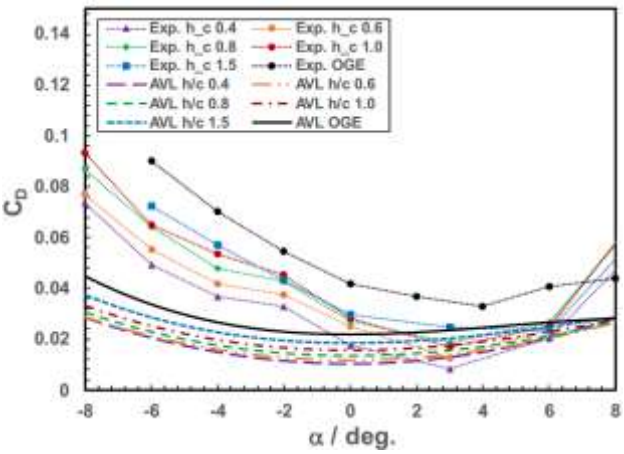


Fig. 11: NACA0012, C_D, experimental vs AVL

The graphs revealed the congruence in the trends between the VLM results and the experimental data for the angles of attack range of interest. There are certainly deviations to be noted, related mostly to the negative angles:

In terms of the lift curves, the experimental data have not captured a substantial increase in the lift curve slope upon varying the h$\bar{c}$/b distance, as

theory would require and evident for the VLM simulations; the almost linear experimentally derived lift coefficient were shown to be transposed upwards rather than having a bigger inclination for smaller values of $h\bar{c}/b$; the VLM results were more congruent with what theory is dictating for the ground effect change in the lift curve slope; at zero angle of attack a more profound positive value for the lift coefficient was captured in the experiments; there are also a less aggressive lift curve slope than the VLM derived ones; for the zero angle of attack cases, the VLM showed a small increase in the lift, if at all, almost indifferent to the $h\bar{c}/b$ distance; for the drag plot, the values spread across tenths of drag counts so the relative importance of properly assessing the drag seems crucial; in general, the experimental data show an aggressive trend for the negative angles of attack and a larger band of spread depending on the $h\bar{c}/b$ distance; it is fair to suggest that the results for drag, whether they have been deducted from the experiments or from the simulations, are to be used only for comparative initial design studies.

3.3 The A-90 Orlyonok Wing Case Study

Following the analytical results correlation and the experimental results benchmark against the VLM computational method for a symmetric rectangular wing, the required adjustments were made to simulate the wing of the A-90 Orlyonok WIG-craft. The geometry of the wing profile and planform of the A-90 Orlyonok was found in [25] and is illustrated in Figure 12 and Figure 13.

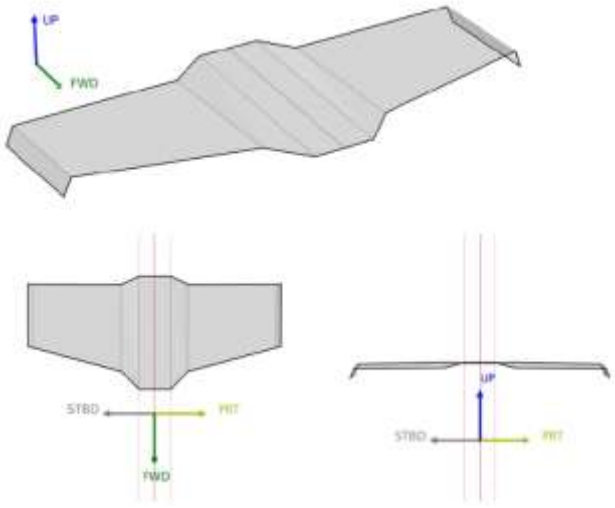


Fig. 12: A-90 Orlyonok 3D wing representation

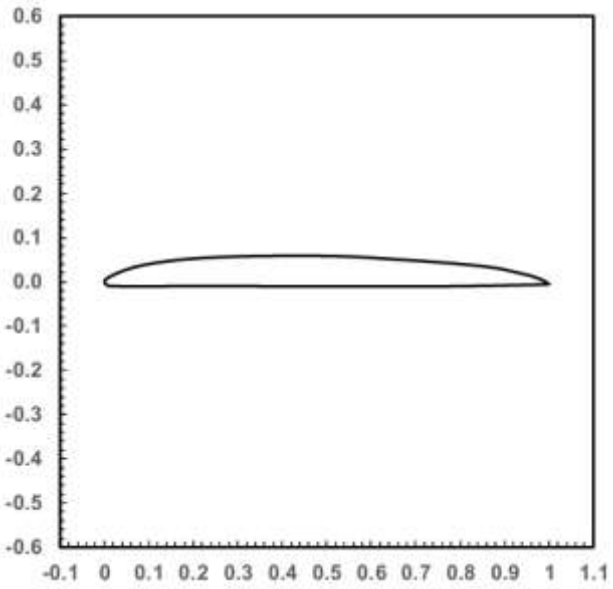


Fig. 13: A-90 Orlyonok 2D normalized chord length wing profile

The analysis flow velocity was set to the Orlyonok's cruise speed of 104 ms^{-1}, [4], while the operational height was set to the typical value of $h\bar{c}/b = 0.4$ for this WIG-craft. Given the differences between the NACA0012 to the A-90 aerofoil profile, area, and operational speed, the impact on wing discretisation was re-assessed. A grid dependence study was conducted for a typical range of angles of attack, with the updated operational parameters and geometry shown in Figure 14, the results of which are presented in Figure 15, Figure 16 and Figure 17.

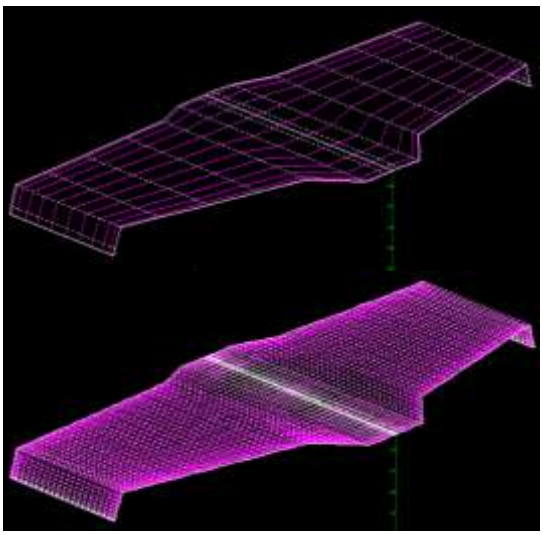


Fig. 14: Mesh sensitivity analysis for the A-90 wing

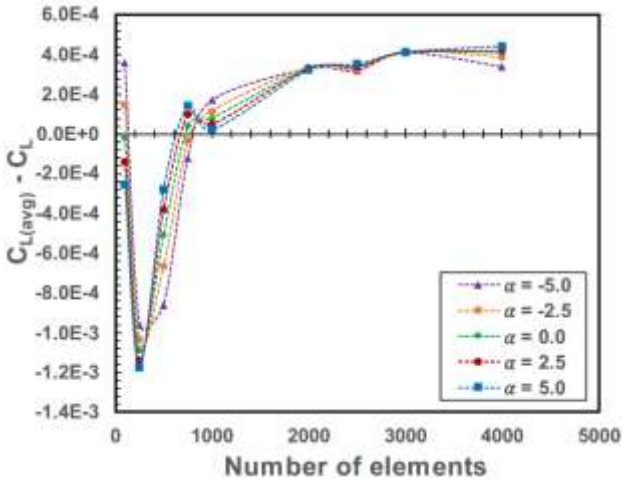


Fig. 15: A-90 3D wing, IGE residuals C_L

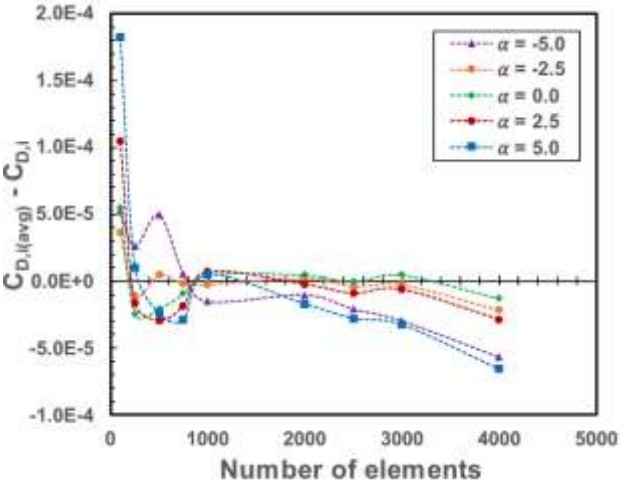


Fig. 16: A-90 3D wing, IGE residuals $C_{D,i}$

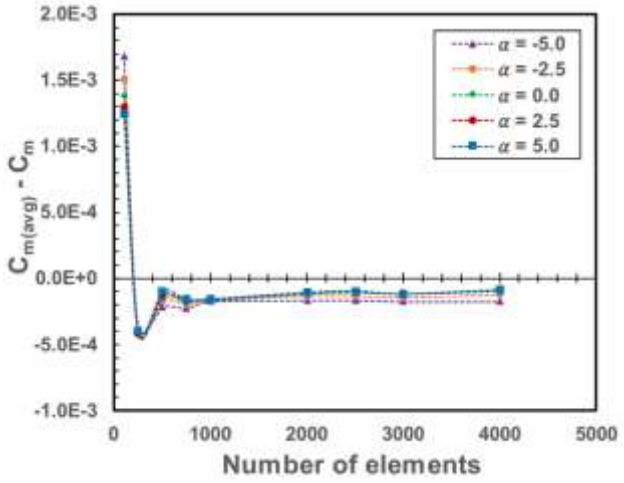


Fig. 17: A-90 3D wing, IGE residuals C_m

The mesh sensitivity analysis showed that the new aerofoil required a significant increase in the number of elements in the grid. The study indicated that a grid with approximately 2000 elements provided results for the lift, drag, and moment coefficients with a maximum error of ± 1% approximately. The proposed grid was considered appropriate for the given purpose to ensure accuracy and reliability for subsequent parametric design analyses.

4 Conclusions

The Vortex Lattice CFD method was used in the present aerodynamic coefficient evaluation study for WIG-craft, where a few hundred simulations were performed efficiently in a relatively short amount of time, concerning higher fidelity CFD methods. The method is ideal for rapid model and results generation, ideal for early design optimization studies. Follow-on research, embedded the Vortex Lattice method within a Python genetic algorithm optimization script, aiming at optimizing the flight performance of WIG-craft, by refining several geometric parameters of various wing design concepts.

The VLM method results for WIG-craft showed a relatively good correlation with the analytic formulations from the public domain, with deviations occurring for closer to the ground distances. The experimental results on the other hand exhibited essential differences in the form of the results generated, not uncommonly met when benchmarking wind tunnel tests against computational methods results. The take-away from the study was that VLM can be used for comparative initial design studies, but flight performance should be judged with higher fidelity computational models and flight testing.

Finally, the study showed that the VLM results convergence does depend on the actual wing design and that there can be an acceptable level of convergence achieved for higher levels of discretization.

References:

[1] Yun L, Bliault A, Doo J, *WIG Craft, and Ekranoplan: Ground Effect Craft Technology*, Springer US, 2010.

[2] Park K, Lee J, Influence of endplate on aerodynamic characteristics of low-aspect-ratio wing in ground effect, *Journal of Mechanical Science and Technology*, 22(12), 2578–2589, 2008.

[3] Rozhdestvensky K, Pappas P, Karaminas E, Stubbs A, Pohl T, Hudson M, Stinton D, Thomasson P, Ekranoplans: The GEMs of Fast Water Transport. Discussion, *Transactions of the Institute of Marine Engineers*, 109(1), 47–74, 1997.

[4] Halloran M, O'meara S, *Wing in Ground Effect Craft Review*. Melbourne Victoria, 1999.

[5] Shirsath R A, Mukherjee R, Experimental and computational investigations of aerodynamic characteristics of a finite rectangular wing-inground effect, *Proceedings of the Institution of Mechanical Engineers, Part G Journal of Aerospace Engineering*, SAGE Publications Ltd, 2022.

[6] Prandtl L, Induced Drag of Multiplanes, *NACA-TN-182*, 1965.

[7] Boschetti P J, Quijada G M, Cárdenas E M, Dynamic ground effect on the aerodynamic coefficients of a wing using a panel method, *AIAA Atmospheric Flight Mechanics Conference. American Institute of Aeronautics and Astronautics Inc.*, 2016.

[8] Suh Y B, Ostowari C O, Drag Reduction Factor Due to Ground Effect, *Journal of Aircraft*, 25(11): 1071–1072, 1988.

[9] Laitone E V, Comment on Drag reduction factor due to ground effect, *Journal of Aircraft*, 27(1): 96–96, 1990.

[10] Phillips W F, Hunsaker D F, Lifting-line predictions for induced drag and lift in ground effect, *31st AIAA Applied Aerodynamics Conference. American Institute of Aeronautics and Astronautics*, 2013.

[11] Chapell P D, Allan J W, Wood S, Low-Speed Longitudinal Aerodynamic Characteristics of Aircraft in Ground Effect, *ESDU 72023*, 2015.

[12] Hoerner S, Borst H, Lift of Airplane Configurations, *Fluid Dynamic Lift*. 2nd ed. Bricktown, NJ: Hoerner Fluid Dynamics, 20.1-20.22, 1985.

[13] Amjad Sohail M, Chao Y, Ullah R, Younis Yamin M, Computational Challenges in High Angle of Attack Flow, *World Academy of Science, Engineering, and Technology,* 56: 1148–1155, 2011.

[14] Anderson R, Willis J, Johnson J, Ning A, Beard R, A comparison of aerodynamic models for optimizing the takeoff and transition of a bi-wing tailsitter, *in AIAA Scitech 2021 Forum. American Institute of Aeronautics and Astronautics Inc*, AIAA, 1–17, 2021.

[15] Kupiainen M, Kreiss G, *Effects of Viscosity on a Shock Wave Solution of the Euler Equations*, in Hou T Y, Tadmor E, (eds) Hyperbolic Problems: Theory, Numerics, Applications. 1st edn. Berlin, Heidelberg: Springer Berlin Heidelberg, 655–664, 2003.

[16] Maier M, Kronbichler M, Efficient Parallel 3D Computation of the Compressible Euler Equations with an Invariant-domain Preserving Second-order Finite-element Scheme, *in ACM Transactions on Parallel Computing. Munich, Germany: Association for Computing Machinery*, 2021.

[17] Kier T M, Verveld M J, Burkett C W, (2015) Integrated Flexible Dynamic Loads Models Based on Aerodynamic Influence Coefficients of a 3D Panel Method, *in International Forum on Aeroelasticity and Structural Dynamics. Saint Petersburg, Russia*, 2015.

[18] Okonkwo P, Jemitola P, *Integration of the athena vortex lattice aerodynamic analysis software into the multivariate design synthesis of a blended wing body aircraft*, Heliyon. Elsevier Ltd, 9(3), 2023.

[19] Solari P, Bagnerini P, Vernengo G, A vortex Lattice Method for the Hydrodynamic Solution of Lifting Bodies Travelling clos and across a free surface, *WSEAS Transaction on Fluid Mechanics,* 17:39-48, 2022.

[20] NASA-AMES WingBody Panel Code, [Online]. https://www.pdas.com/wingbody.html, (Accessed Date: February 5, 2024).

[21] The PANAIR Program for Panel Aerodynamics, [Online]. https://www.pdas.com/panair.html, (Accessed Date: February 5, 2024).

[22] XFLR5, [Online]. http://www.xflr5.tech/xflr5.htm, (Accessed Date: February 5, 2024).

[23] Drela M, Youngren H, AVL, [Online]. https://web.mit.edu/drela/Public/web/avl/, (Accessed Date: February 5, 2024).

[24] Wieselberger C, Wing Resistance near the Ground, (Uber den Flügelwiderstand in der Nahe des Bodens, *Zeitschift für Flugtechnik und Motorluftschiffahrt) Magazine for aviation technology and motor aviation*, 25(11): 145–147, 1921.

[25] Мараев Р, Flying over the waves (Ekranoplan 'Eaglet') 1992, [Online]. http://www.razlib.ru/transport_i_aviacija/ayerohobbi_1992_02/p3.php, (Accessed Date: February 5, 2024).

Contribution of Individual Authors to the Creation of a Scientific Article (Ghostwriting Policy)

- Karl Zammit: methodology, investigation, formal analysis, software, validation, project administration.
- Howard Smith: conceptualization, supervision, project administration.
- Noel Sierra Lobo: investigation.
- Ioannis K. Giannopoulos: validation, visualization, writing.

Sources of Funding for Research Presented in a Scientific Article or Scientific Article Itself

No funding was received for conducting this study.

Conflict of Interest

The authors have no conflicts of interest to declare that are relevant to the content of this article.

Creative Commons Attribution License 4.0 (Attribution 4.0 International, CC BY 4.0)

This article is published under the terms of the Creative Commons Attribution License 4.0
https://creativecommons.org/licenses/by/4.0/deed.en_US



https://dspace.org/

Vortex lattice CFD application and modeling validation for ground effect aircraft

Zammit, Karl; Smith, Howard; Lobo, Noel Sierra; Giannopoulos, Ioannis K.

2024-02-09
WSEAS (World Scientific and Engineering Academy and Society)
https://doi.org/10.37394/232013.2024.19.5
Zammit K, Smith H, Lobo NS et al., (2024) Vortex lattice CFD application and modeling validation for ground effect aircraft. WSEAS Transactions on Fluid Mechanics, Volume 19, February 2024, Article number 5, pp. 49-58

Downloaded from a DSpace repository. https://dspace.org/